Biomedicine & Pharmacotherapy 170 (2024) 115981

Contents lists available at ScienceDirect

Biomedicine & Pharmacotherapy

journal homepage: www.elsevier.com/locate/biopha

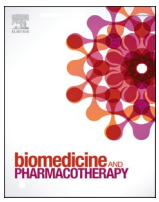

siRNA lipid nanoparticles for CXCL12 silencing modulate brain immune response during Zika infection

Pedro Augusto Carvalho Costa [a], Walison Nunes da Silva [a], Pedro Henrique Dias Moura Prazeres [a,b], Heloísa Athaydes Seabra Ferreira [a], Natália Jordana Alves da Silva [a], Maria Marta Figueiredo [c], Bruna da Silva Oliveira [d], Sérgio Ricardo Aluotto Scalzo Júnior [a], Felipe Rocha da Silva Santos [e], Rúbia Aparecida Fernandes [d], Rohan Palanki [f], Alex G. Hamilton [f], Alexander Birbrair [g], Victor Rodrigues Santos [d], Aline Silva de Miranda [d], Michael J. Mitchell [f], Mauro Martins Teixeira [e], Vivian Vasconcelos Costa [d], Pedro Pires Goulart Guimarães [a,*]

[a] Department of Physiology and Biophysics, Institute of Biological Sciences, Federal University of Minas Gerais, Belo Horizonte 31270-901, MG, Brazil
[b] Department of General Pathology, Federal University of Minas Gerais, Belo Horizonte, MG, Brazil
[c] State University of Minas Gerais, Divinopolis 35501-170, Brazil
[d] Department of Morphology, Federal University of Minas Gerais, Belo Horizonte, Minas Gerais 31270-901, Brazil
[e] Department of Biochemistry and Immunology, Federal University of Minas Gerais, Belo Horizonte, Minas Gerais 31270-901, Brazil
[f] Department of Bioengineering, University of Pennsylvania, Philadelphia, PA, 19104-6321, United States
[g] Department of Dermatology, University of Wisconsin-Madison, WI 53706, United States

ARTICLE INFO

Keywords:
Neuroimmunomodulation
CXCL12
Zika virus
Lipid nanoparticle
siRNA

ABSTRACT

CXCL12 is a key chemokine implicated in neuroinflammation, particularly during Zika virus (ZIKV) infection. Specifically, CXCL12 is upregulated in circulating cells of ZIKV infected patients. Here, we developed a lipid nanoparticle (LNP) to deliver siRNA in vivo to assess the impact of CXCL12 silencing in the context of ZIKV infection. The biodistribution of the LNP was assessed in vivo after intravenous injection using fluorescently tagged siRNA. Next, we investigated the ability of the developed LNP to silence CXCL12 in vivo and assessed the resulting effects in a murine model of ZIKV infection. The LNP encapsulating siRNA significantly inhibited CXCL12 levels in the spleen and induced microglial activation in the brain during ZIKV infection. This activation was evidenced by the enhanced expression of iNOS, TNF-α, and CD206 within microglial cells. Moreover, T cell subsets exhibited reduced secretion of IFN-ɣ and IL-17 following LNP treatment. Despite no observable alteration in viral load, CXCL12 silencing led to a significant reduction in type-I interferon production compared to both ZIKV-infected and uninfected groups. Furthermore, we found grip strength deficits in the group treated with siRNA-LNP compared to the other groups. Our data suggest a correlation between the upregulated pro-inflammatory cytokines and the observed decrease in strength. Collectively, our results provide evidence that CXCL12 silencing exerts a regulatory influence on the immune response in the brain during ZIKV infection. In addition, the modulation of T-cell activation following CXCL12 silencing provides valuable insights into potential protective mechanisms against ZIKV, offering novel perspectives for combating this infection.

1. Introduction

Zika virus (ZIKV) is a flavivirus that can cause neuropathogenesis in adults and fetal central nervous system (CNS) malformation following infection in pregnant women [1–4]. ZIKV infection was declared a global disease after its outbreak in 2016 [5]. The mechanisms underlying ZIKV pathogenesis remain poorly understood and seem to involve a complex interplay between viral and host factors [6]. ZIKV has been shown to modulate both the innate and adaptive immune response to escape and trigger neuropathogenesis [2,3,7,8,9]. ZIKV-induced

* Corresponding author.
E-mail address: ppiresgo@reitoria.ufmg.br (P.P.G. Guimarães).

https://doi.org/10.1016/j.biopha.2023.115981
Received 9 October 2023; Received in revised form 28 November 2023; Accepted 2 December 2023
Available online 12 December 2023

neuropathogenesis involves the activation of immune and inflammatory responses initiated by local and infiltrated glial cells, including microglia and astrocytes, as well as immune cells such as peripheral macrophages and lymphocytes within the brain[10]. Microglial cells are the first defense during viral infection of the brain parenchyma [11].

CXCL12 is a chemokine that is constitutively expressed in a variety of tissues, including the liver, spleen, brain, and kidneys. CXCL12 has been found to be systemically upregulated in monocytes of patients infected with ZIKV [12]. In addition, it has been demonstrated that ZIKV infection results in specific short- and long-term enhanced expression of CXCL12 in the central nervous system (CNS) and it persists long after the initial viral infection is cleared [13].

Small interfering RNA (siRNA) is a therapeutic approach to silence the expression of specific endogenous. siRNA is unstable in the bloodstream and requires a delivery method to bypass cell membranes [14]. Lipid nanoparticles (LNPs) have been developed to encapsulate nucleic acids to avoid degradation and mediate their intracellular delivery [15]. Of note, recent examples reinforce the potential use of LNP for nucleic acid delivery such as the FDA-approved LNP-based siRNA developed by Alnylam Pharmaceuticals, and the FDA-approved NP-based mRNA vaccines against COVID-19, developed by Moderna and Pfizer/BioNTech [16].

Here, we developed a lipid nanoparticle (LNP) to deliver siRNA in vivo to assess the effect of CXCL12 silencing during ZIKV infection and its implications in neuropathology. We showed that silencing CXCL12 in the spleen was able to modulate microglia and lymphocyte activation in the brain, which resulted in decreased limb strength without changes in viral load. Together, our results demonstrate that CXCL12 silencing modulates brain immune response during ZIKV infection.

2. Materials and methods

2.1. Polymer-lipid synthesis

In this study, we synthesized hybrid polymer-lipids using a previously reported method [17]. Briefly, the polymer-lipids were synthesized by reacting low molecular PEI (Sigma-Aldrich, St. Louis, MO, US) with C15 epoxide terminated alkyl tails (Tokyo Chemical Industry, Tokyo, Japan) at 90 ºC in 100% ethanol for 48 h at a 14:1 molar ratio. Polymer-lipids were purified via flash chromatography to isolate the optimized hydrophobic C15:hydrophilic PEI.

2.2. siRNA Nanoparticle Formulation

The LNPs were formulated using a microfluidic mixing method to combine polymer-lipid (7C1) and modified PEG-lipid with siRNA. Briefly, the 7C1, and 1,2-dioleoyl-sn-glycero-3-phosphoethanolamine-N-[methoxy(polyethylene glycol)− 5000] (ammonium salt) (C18-PEG 5000, Avanti Polar Lipids, no. 880230) were solubilized in ethanol at a final concentration of 10 mg/mL and 12.5 mg/mL, respectively. siCXCL12 was solubilized in 10 mM citrate buffer, pH 3.0 (Teknova, Hollister, CA, US). Ethanol and aqueous phases were mixed using a microfluidic device at a 1:3 ratio (ethanol:aqueous phase) and the LNPs were collected into a 20 MWCO dialysis cassettes (Thermo Scientific). NPs were dialyzed against PBS 1x, pH 7.4 for 2 h and sterile filtered through 0.22 μm syringe filters before in vivo experiments. To prepare fluorescent NPs, siRNA labeled with fluorescent Alexa Fluor 647 dye was used, following the same protocol.

2.3. Characterization of LNP

LNP were characterized by their hydrodynamic diameter (HD), polydispersity index (PDI), and zeta potential (ZP) measured using a Zetasizer Nano ZS machine (Malvern Panalytical). The LNP structure was investigated using cryogenic-transmission electron microscopy (cryo-TEM). LNPs samples were prepared in a vitrification system (25 °C, ~100% humidity) and examined using Tecnai G2–20 - FEI SuperTwin 200 kV at the Center for Acquisition and Processing of Images (Centro de Aquisição e Processamento de Imagens - UFMG). siRNA quantification and encapsulation efficiency were measured using both Quant-iT™ RiboGreen (Invitrogen) and NanoDrop Spectrophotometer (Thermo Scientific).

2.4. Biodistribution assay

To investigate the LNPs biodistribution, we used LNP encapsulated with fluorescent siRNA (Alexa Fluor 647). The siRNA-LNPs were intravenously injected in C57BL/6 mice (n = 4) and tissues were harvested 6 h later and the fluorescence was assessed via IVIS Imaging System (Perkin-Elmer). The fluorescence was quantified by Living Image Software (Perkin-Elmer) as total radiant efficiency.

2.5. ZIKV and cells

For in vivo experiments, we used the Zika virus (ZIKV) strain HS-2015-BA-01 (GenBank KX520666), which was originally isolated in 2015 from a symptomatic patient in Bahia State. The ZIKV stocks were propagated in mycoplasma-free Vero cells and the viral titer in the tissues was determined by plaque assay. Results were measured as a plaque forming units (PFU) per gram of tissue weight [18]. All experiments with ZIKV were conducted under biosafety level 2 (BSL2) containment at Federal University of Minas Gerais (UFMG).

2.6. In vivo experiments

To perform in vivo experiments we used A129 mice deficient in type I interferon receptor (IFN-α/βR−/−) on SV129 background [19]. Adult mice (7–9 weeks old) were kept under specific-pathogen-free conditions. For the experiments, mice were inoculated with 4×10^3 PFU ZIKV via intravenous (i.v.) injection. All animal care and experimental procedures were approved by the Ethics Animal Care and Use Committee (CEUA - 272/2022), in accordance with the Guide for the Care and Use of Laboratory Animals from the UFMG.

2.7. siCXCL12-LNP silencing IFN-α/βR− /− mice during ZIKV infection

To assess the in vivo effect of siCXCL12-LNPs during ZIKV infection, mice were treated 2 days post-infection with ZIKV using 2 mg/kg of siCXCL12 encapsulated in LNP (siCXCL12-LNP) every day for 4 days via intravenous route. Clinical signs (presence of ruffled fur, partial or complete hind limb weakness or paralysis, and loss in body weight) were monitored daily.

Hematological analysis. Blood samples were collected from the cheek using heparin-containing syringes on the sacrifice day. Total and differential leucocyte counts were determined by using a hemocytometer.

2.8. qRT-PCR

To investigate IFN-β expression in the brain after CXCL12 silencing during ZIKV infection, we performed quantitative reverse transcription polymerase chain reaction (qRT-PCR). Total RNA was extracted using Trizol, according to the manufacturer's instructions, and quantified using Nanodrop Lite (Thermo Fischer Scientific). High-Capacity cDNA Reverse Transcription Kit (Thermo Fisher Scientific) was used for first-strand cDNA synthesis (Reverse Transcriptase (RT)) from 1 μg of total RNA. Reverse transcription products were diluted and submitted to qRT-PCR (0.5 ng of cDNA/reaction) using PowerUp SYBR Green Master Mix (Applied Biosystems). The PCR steps were as follows: 95 °C – 10 min, followed by 40 cycles of 95 °C – 15 s; 60 °C – 1 min, and 72 °C – 20 s, and the reactions were performed in QuantStudio 3 (Applied Biosystems). Specific primers were IFN-β forward 5' CAGCTCCAAGAAAGGACGAAC

3' and reverse 5' GGCAGTGTAACTCTTCTGCAT 3'. Ct values were recorded for each gene and the results were normalized using the S26 housekeeping gene. The efficiency and slope values were close to the optimal values required for the ΔΔCT analysis for all investigated candidate genes [20].

2.9. Histopathological and immunofluorescence analysis

To investigate the brain damage and activated microglia, we performed histopathology and immunofluorescence analysis. Mice were anesthetized and perfused with saline followed by 4% buffered paraformaldehyde (PFA, pH = 7.4). For histopathological studies, brain and liver were harvested and embedded in paraffin, sectioned at 3–5 μm thick and stained with hematoxylin and eosin (H&E). Histech 3D Slide Scanner was used for a fast scan of slides. For immunofluorescence, tissues were fixed overnight with 4% PFA at 4 °C. Next, tissues were subjected to a sucrose gradient in PBS, first at 10% sucrose, then 15% sucrose, each for one hour at 4 °C. Then, tissues were incubated overnight at 4 °C in 30% sucrose solution. Tissues were embedded and frozen in an optimal cutting temperature compound (OCT, Tissue-Tek). 20 μm cryosections were prepared and blocked for 2 h in 3% BSA in PBS + 0.5% Triton. Samples were stained with antibodies against ionized calcium-binding adaptor molecule 1 (Iba1) (dilution 1:100) (Cat# PA5–21274, Life Technologies), CD68 (dilution 1:100) (Cat# ab125212, Abcam), and S100b (dilution 1:100) (Cat# ab41548, Abcam), with goat anti-rabbit AlexaFluor-647 (1:1000; A21245) (Life Technologies) and goat anti-rabbit Alexa 488 (1:1000; A-11034) (Life Technologies) used as secondary stains. Sections were washed with PBS containing 4',6-diamidino-2-phenylindole (DAPI, 5 μg/mL, Invitrogen) and mounted using Dako fluorescence mounting medium (Dako, Santa Clara, CA). Images were taken using Zeiss LSM 880 microscope (Oberkochen, Germany). The number of $Iba1^+$, $CD68^+$, $Iba1^+CD68^+$ and $S100b^+$ cells were quantified using Fiji software, version 1.53 (National Institute of Health). Multiple random fields of each section were used for quantification and the size of cell bodies was measured [21].

2.10. Brain-infiltrating cells immunophenotyping and intracellular cytokine measurement

To assess the immunophenotyping of infiltrating cells and intracellular cytokine measurements, brain tissues were harvested after perfusion with PBS and kept on ice. Harvested brains were macerated and filtrated through cell strainers (70 μm) to perform brain and liver cell enrichment with a 35% and 37% Percoll (Sigma Aldrich) gradient, respectively, for immunophenotyping [22,23]. Antibodies used are listed in Table S1. CountBright™ Absolute Counting Beads were used for flow cytometry for cell numbers (ThermoFisher). Dead cells were excluded using Live/Dead (Invitrogen) for further labeling of extracellular and intracellular antigens after fixation and permeabilization (FoxP3 staining buffer set, eBioscience) according to the manufacturer's instructions. LSR-FORTESSA equipment was used on acquisition. Data were analyzed by excluding debris, removing doublets with a forward scatter area (FSC-A) versus forward scatter height (FSC-H) gate, to avoid interruptions in the flux. Cells were gated in the function of time versus FSC-A. Only live CD45-intermediate and CD45-high cells were used, and different subpopulations based on cell markers were evaluated (Table S1). IFN-γ, IL-17, IL-10, TNF-α, and iNos production were measured in each cell subset of brain microenvironment using intracellular staining. Also, CXCL12 expression was evaluated in brain, liver, and spleen cells. Isolated brain cells were cultivated overnight to assess cytokines at 37 °C in 10% FBS RPMI supplemented with 2 mM L-glutamine, 50 units/mL penicillin, and 50 μg/mL streptomycin, in the presence of Brefeldin A (ThermoFisher). GraphPad Prism V7.0 (GraphPad software) and FlowJo V10.4.11 (BD) were used for data analysis. Cytofikit 2 was used for the dimensionality reduction and visualization by Uniform Manifold Approximation and Projection (UMAP). Guided FlowSom was used for clusterization. In the UMAP analysis, every experimental group consists of eight mice, with an equal number of cells used as input.

2.10.1. Behavioral tests

Open-field test was carried out to determine general activity levels in mice. In the afternoon, the animals were transferred to the testing room, where the experimental setup was situated. The animals were provided with food and water and not subjected to any deprivation before the test. A habituation phase of 30 min was allowed, following which the animals were introduced into the PhenoTyper® System (Noldus Information Technology, Leesburg, VA, United States) and allowed to explore the opaque plastic arena (measuring 30 × 30 cm) freely for 30 min. The total distance traveled by the animals (in centimeters) was quantified using the Ethovision XT software (Noldus Information Technology, Leesburg, VA, United States). Furthermore, grip strength of the forelimbs was evaluated. Animals were gently lowered onto the grip strength bar and allowed to hold on before being pulled horizontally by their tails. The test was terminated once the animal released its grip, and the mouse was then placed in a large plexiglass bucket containing bedding. The force exerted at the point of release was measured in Newtons (N), and three pulls per mouse were recorded. In the analyses, an average was calculated across each genotype and treatment condition.

2.11. Statistical analysis

Data are presented as mean ± SD. Student's t-test, Mann-Whitney test, one-way or two-way analysis of variance (ANOVA) followed by the Tukey or Dunnett's post hoc test was applied for comparison between two groups or among multiple groups using Graphpad Prism 7.0, respectively. Outliers were removed using Grubbs's test and statistical normality was verified by D'Agostino-Pearson's K^2 test. Differences were considered statistically significant for * $.01 < p < .05$; * *$.001 < p < .01$; * ** $p < .001$ and * ** * $p < .0001$.

3. Results

3.1. Characterization and in vivo biodistribution of LNPs

We formulated a lipid nanoparticle (LNP) to effectively deliver siRNA in vivo to silence CXCL12 during ZIKV infection. To formulate the LNP, termed siCXCL12-LNP, we utilized a microfluidic device to mix an ethanol phase containing a hybrid polymer-lipid and an aqueous phase of siRNA (Fig. 1 A). The size, polydispersity, and zeta potential of the LNPs were assessed by dynamic light scattering (DLS) and transmission electron microscopy (Cryo-TEM), and zeta potential (ZP). The size of the siCXCL12-LNP varied from 104 to 110 nm (Fig. 1B) while the PDI was less than 0.2 (Fig. 1B), indicating low polydispersity of this LNP. Cryo-TEM results confirmed that homogenous siCXCL12-LNP was formed with a spherical morphology (Fig. 1 C). Furthermore, the ZP values of the siCXCL12-LNP were negative and ranged between − 2.52 mV to − 8.93 mV (Fig. 1D). To evaluate in vivo biodistribution, a fluorescent siRNA was encapsulated in the LNP and the formulation was injected via intravenous injection into A129 mice. Six hours post-administration, animals were sacrificed, and organs were harvested for analysis via and IVIS imaging system (Fig. 1E). Fluorescence was significantly higher in the liver and spleen compared to other tissues such as the lung (Fig. 1 F), which is suggestive of substantial siRNA accumulation in the liver and spleen.

3.2. In vivo CXCL12 silencing using LNP

To assess in vivo CXCL12 silencing, A129 mice were treated starting 2 days post-infection with ZIKV using 2 mg/kg of siCXCL12 encapsulated in LNP (siCXCL12-LNP) every day for 4 days via intravenous injection (Fig. 2 A). ZIKV infection significantly increased levels of

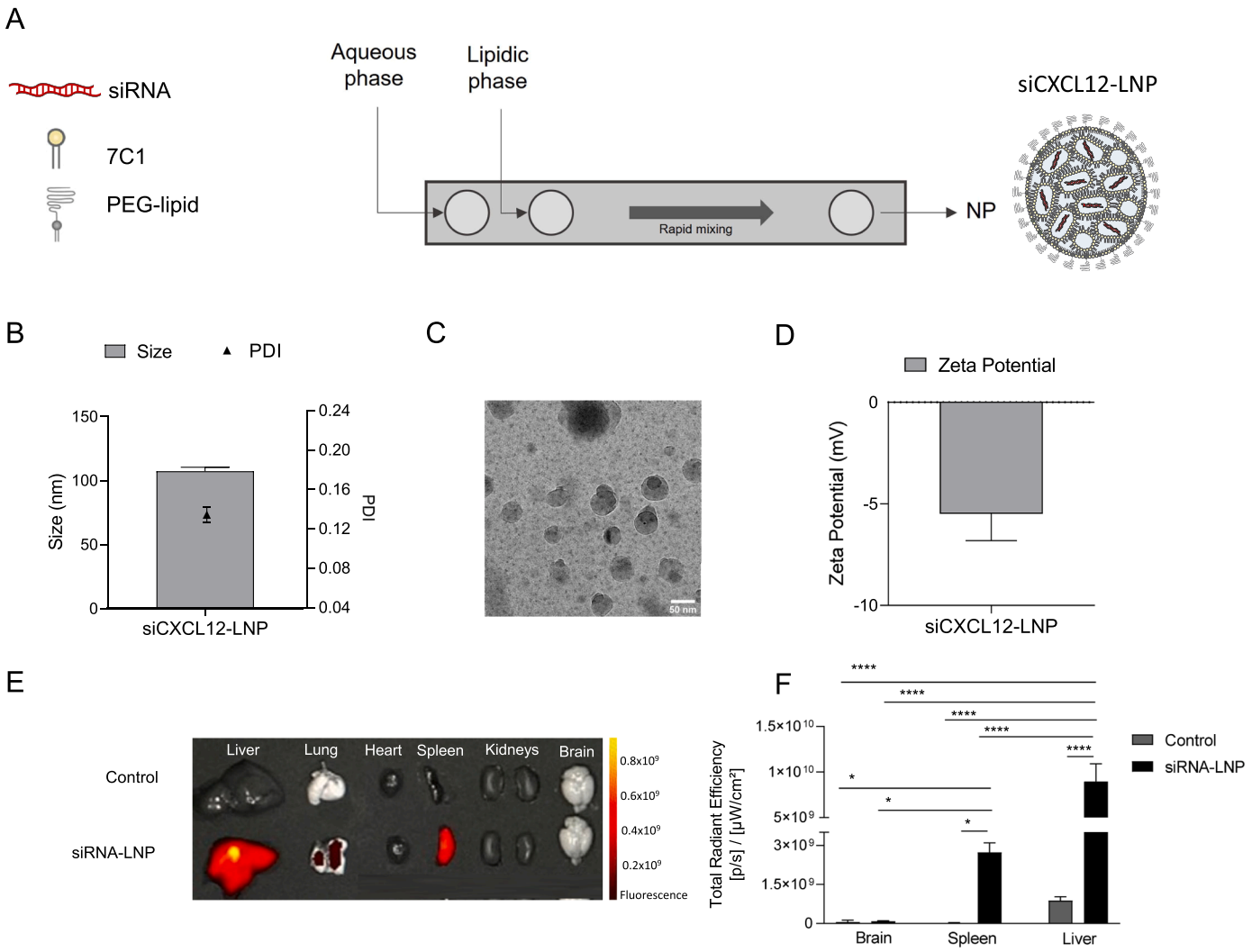

Fig. 1. Characterization of LNPs encapsulating siRNA for CXCL12 silencing. (A) Schematic representation of components to formulate LNPs via microfluidic mixing. (B) Hydrodynamic diameter measurements and polydispersity index (PDI) of LNPs. Bar graph: size; Bar dot: PDI. (C) Representative cryogenic-transmission electron microscopy of LNPs encapsulating siRNA (siCXCL12-LNP; scale bar = 100 nm). (D) Zeta potential demonstrated slightly negatively charged siCXCL12-LNPs. (E) Representative images of LNP delivery in different organs via fluorescence detection. (F) Quantification of fluorescence in brain, liver and spleen 6 h after treatment with nanoparticles encapsulated with fluorescent siRNA. Data are presented as mean ± SD. One-way ANOVA followed by Tukey's multiple comparison and Two-way ANOVA followed by Tukey's multiple comparison test (F); * $p < 0.05$, * * $p < 0.01$.

CXCL12 expression in CD11b+ cells isolated from the brain and the spleen but not the liver (Fig. 2B-D). Importantly, treatment of ZIKV infected mice with siCXCL12-LNP resulted in a significant decrease in CXCL12 expression in CD11b+ cells isolated from the spleen (Fig. 2 C). Changes in CXCL12 expression were not observed in CD11b+ cells from the brain or the liver (Figs. 2B, 2D).

Next, we assessed clinical signs of ZIKV infection in mock, mock +siCXCL12-LNP, ZIKV, and ZIKV+siCXCL12-LNP groups via a previously-validated scoring matrix [24]. As expected, compared to uninfected animals, both ZIKV-infected cohorts displayed clinical signs of ZIKV infection and correspondingly higher clinical scores (Fig. 2E). In addition, ZIKV-infected cohorts – with and without siCXCL12-LNP treatment – had increased total leukocytes in the blood (Fig. 2 F) and greater numbers of granulocytes and lymphocytes compared to uninfected groups (Fig. 2 G). However, there was no significant changes to both clinical score and number of immune cells between the ZIKV-infected group and the siCXCL12-LNP treated ZIKV-infected group (Fig. 2 F, 2 G).

We also investigated damage to brain tissue in histological sections from animals in each experimental group. While there was no brain damage in the mock and mock+siCXCL12-LNP groups, we observed intense inflammatory infiltration in the ZIKV and ZIKV+siCXCL12-LNP groups (Fig. 2H). There were no significant differences in gross damage to the brain or liver between ZIKV and ZIKV+siCXCL12-LNP groups (Fig. 2H and Fig. S1) nor absolute number of $CD45^+$ cells infiltrated in the brain (Fig. 2I). Taken together, these results indicate that while siCXCL12-LNPs were safe, they did not result in ZIKV-mediated pathology.

3.3. Glial components are activated after CXCL12 silencing during ZIKV infection

An additional experimental cohort of mice – infected and treated in a similar manner – was followed to assess the effect of CXCL12 silencing on glial cell activation (Fig. 3 A). To investigate microglial reaction in harvested mouse brains, we evaluated the expression of microglial markers Iba1 and CD68 using confocal laser scanning microscopy. Although there were no differences in the Iba1 expression between groups (Fig. 3B, C), we found increased number of $CD68^+$ (Fig. 3B, D) and $Iba1^+CD68^+$ (Fig. 3B, E) cells in the ZIKV+siCXCL12-LNP group compared to ZIKV and uninfected mock group. However, there was no difference in number of $S100b^+$ cells (mature astrocytes) after treatment

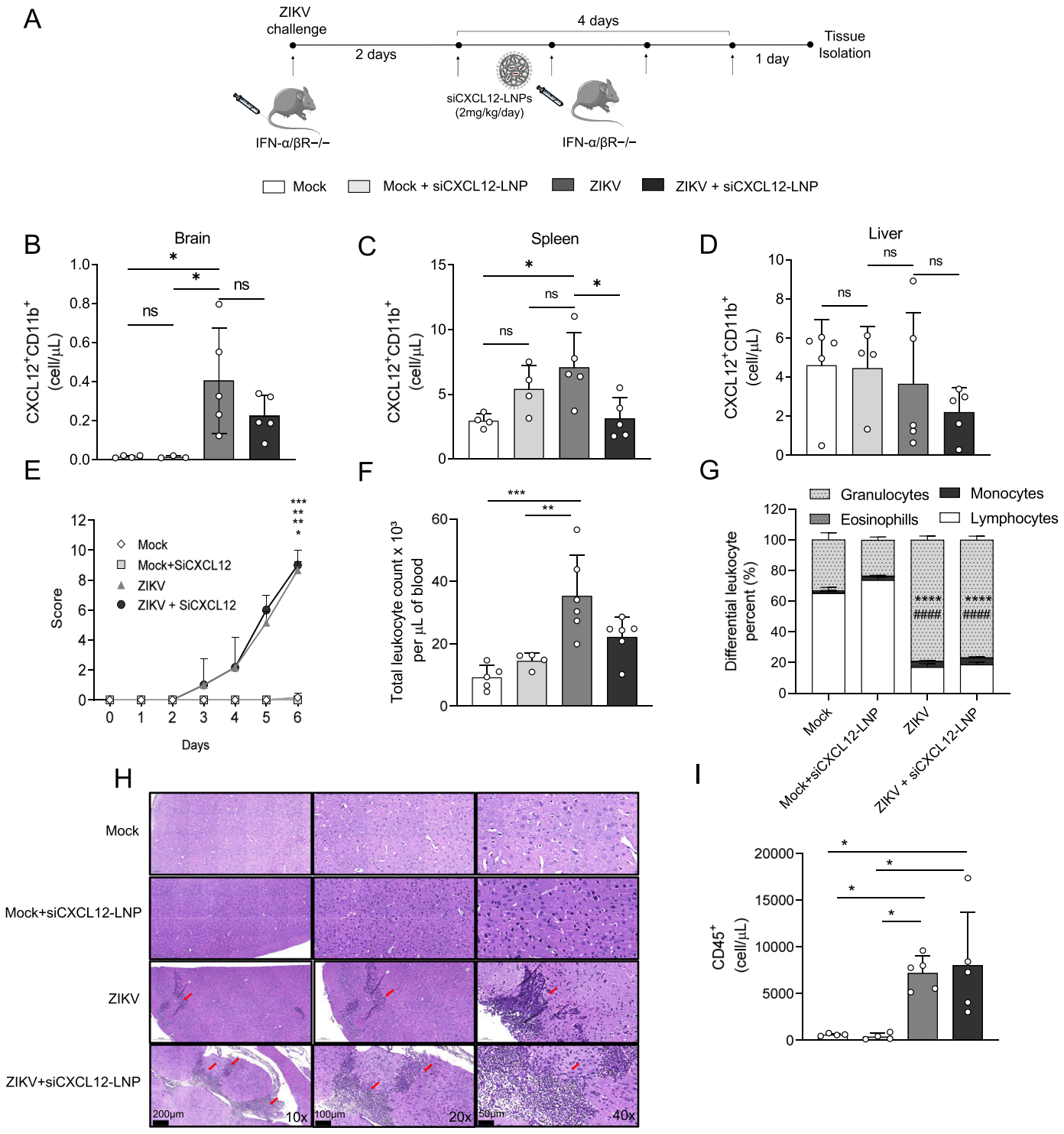

Fig. 2. In vivo CXCL12 silencing using LNP (A) Scheme of infection with ZIKV and treatment with siCXCL12-LNPs. CXCL12 production by $CD11b^{+}$ cells of uninfected mice (mock group), uninfected mice treated with siCXCL12-LNP (mock+siCXCL12-LNP), infected mice with ZIKV (ZIKV group) and infected mice with ZIKV treated with siCXCL12-LNP (ZIKV+siCXCL12-LNP group) in (B) brain, (C) spleen, and (D) liver (n = 20). (E) Score of mice inoculated i.v. with 4×10^5 PFU of the Brazilian strain of ZIKV (HS-2015-BA-01). (F) Total leukocytes 6 days post-infection with ZIKV; (G) Differential blood cell counts, represented as the number of differential cell counts (granulocytes, eosinophils, monocytes, and lymphocytes) normalized by the percentage of the total cell count 6 days post-infection with ZIKV. (H) Histopathological analysis at 10x, 20x, 40x magnification of the brain at 6 days post-infection with ZIKV ($n = 5$/group). Data are presented as mean ± SD. (B, C, D, F, I) One-way ANOVA followed by Tukey's multiple comparison. (E, G) Two-way ANOVA followed by Tukey's multiple comparison test. * .01 < p < .05, * *.001 < p < .01, * ** p < .001, and * ** * p < .0001.

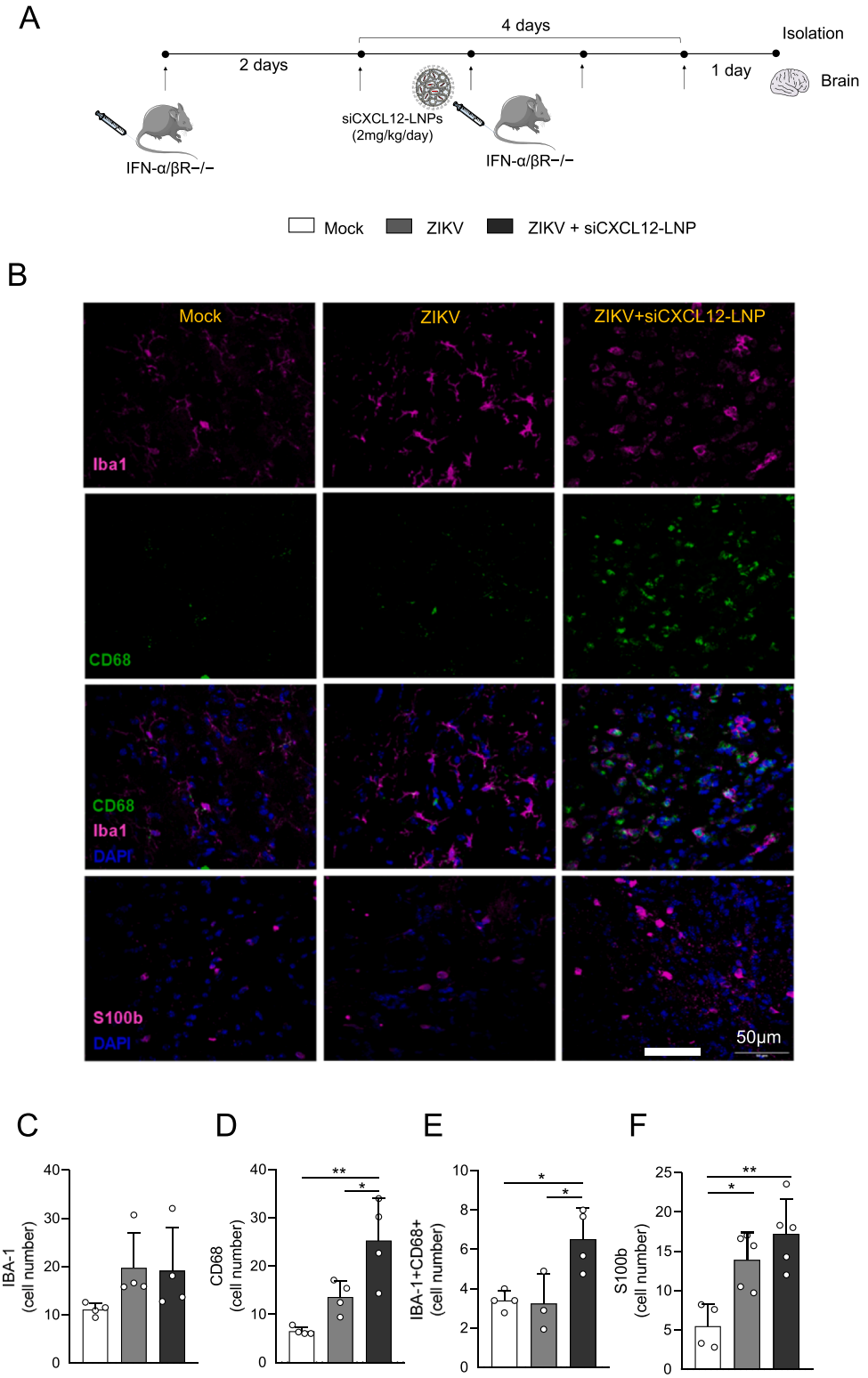

Fig. 3. CXCL12 modulates microglia activation triggered by ZIKV infection. (A) Scheme of infection with ZIKV and treatment with siCXCL12-LNPs. (B) Representative immunofluorescence images of brains labeled for IBA (purple), CD68 (green), IBA+CD68 +DAPI (DAPI; blue), and S100b+DAPI (S100b; purple), from mock, ZIKV and ZIKV+siCXCL12-LNP groups of IFN-α/βR− /− mice (n = 15). Graphs from (C) IBA, (D) CD68, (E) IBA+CD68 +DAPI and (F) S100b+DAPI. Data are presented as mean ± SD. One-way ANOVA followed by Tukey's multiple comparison test; * .01 < p < .05, * *.001 < p < 0.01, * ** p < 0.001, and * ** * p < 0.0001.

with siCXCL12-LNP in comparison to mock and ZIKV groups (Fig. 3B, F). The cells labeled with Iba-1/CD68+ also revealed changes in the size of cell bodies. Specifically, increased size of cell bodies was found in the ZIKV+siCXCL12-LNP group compared to ZIKV and mock groups. (Fig. S2A). On the hand, it was not observed changes between groups in the size of cell bodies of astrocytes labeled with S100b (Fig. S2B).

In addition, we investigated activated microglia in harvested mouse brains using flow cytometry. Representative density plots demonstrating the gating strategy used for activated microglial cells ($CD45^{int}CD11b^{+}F4/80^{+}MHCI^{+}$) are shown in Fig. 4B [25]. Increased $CD45^{int}$ subset (Fig. 4 C) and activated microglia (Fig. 4D) prevalence were found in the ZIKV+siCXCL12-LNP group compared to mock group. To assess the pattern of inflammation, we next characterized the expression of the mannose receptor (CD206+) and different cytokines in these activated glial cells. ZIKV infection enhanced TNF-α cytokines compared to mock group, as expected. Importantly, the group treated with siCXCL12-LNP (ZIKV+siCXCL12-LNP) significantly enhanced not only the number of $CD206^{+}$ microglial cells but also the iNOS and TNF-α cytokines, compared to both mock and ZIKV groups. IL-10, an anti-inflammatory cytokine, was also increased in ZIKV and ZIKV+siCXCL12-LNP groups compared to mock (Fig. 4E - H). Furthermore, UMAP analysis revealed the presence of distinct cell populations based on CD206 expression in Mock, ZIKV and ZIKV+siCXCL12-LNP groups. While it was observed subsets with enhanced CD206 expression and low iNOS and TNF-α levels in ZIKV, and ZIKV+siCXCL12-LNP groups, we found subsets with low CD206 expression associated with high iNOS and TNF-α in the same groups (Fig. 4I). On the other hand, we did not observe changes in cytokine production by monocytes, macrophages, and dendritic cells in the group treated with siCXCL12-LNP compared to mock and ZIKV groups (Fig. S3A-O). Together, these results suggest that microglial cells are activated in the brain after CXCL12 silencing, which leads to enhanced production of inflammatory cytokines.

3.4. Lymphocyte activation is dependent of CXCL12 during ZIKV infection

A third experimental cohort of mice – infected and treated in a similar manner – was followed to assess the effect of CXCL12 silencing on lymphocyte activation (Fig. 5 A). CXCL12 mediates the chemoattraction of T cells and enhances the stimulation of T cells through the T cell receptor (TCR) [26]. Thus, we assessed the lymphoid cells in harvested mouse brains after treatment with siCXCL12-LNP via flow cytometry. We found significantly increased levels of $CD4^{+}$, $CD8^{+}$, $CD4^{-}CD8^{-}$, and NKT cells (Fig. 5B-F) as well as of NK and T_{reg} cells (Fig. S4A-F) after ZIKV infection compared to mock. Although the numbers of these cells were not altered by the treatment with siCXCL12-LNP, IFN-ɣ production was significantly decreased in CD4 and NKT subpopulations of ZIKV+siCXCL12-LNP group compared to ZIKV group (Fig. 5G-J). Enhanced levels of IL-17 in CD4, CD8, $CD4^{-}CD8^{-}$, and NKT subsets (Fig. 5K-N) in the untreated ZIKV group were normalized to near baseline after treatment of infected mice with siCXCL12-LNP (ZIKV+siCXCL12-LNP group) (Fig. 5K-N). While ZIKV infection inhibited type-I interferon production [27,28], treatment with siCXCL12-LNP resulted in additional decreased type-I interferon levels (Fig. 4 O).

3.5. Viral load was not changed during CXCL12 silencing

To investigate viral load after treatment with siCXCL12-LNP, experimental mouse brains and serum were collected to perform a gold-standard plaque assay for viral load. We haven't found significant differences in viral load between ZIKV+siCXCL12-LNP and ZIKV groups in the brain and serum (Fig. 5 P, Q).

3.6. Effect of CXCL12 on motor behavior during ZIKV infection

To investigate the animal behavior after CXCL12 silencing during ZIKV infection, grip strength and open field tests were performed. Although we did not observe changes in locomotor activity in the open field, we found significant grip strength deficits in the ZIKV+siCXCL12-LNP group compared to mock and ZIKV groups (Fig. 6 A-B).

4. Discussion

ZIKV can infect and replicate in primary undifferentiated neurons and trigger neuronal killing [10]. CXCL12 plays a key role in mediating, among other functions, leukocyte trafficking through the BBB [29]. The chemokine CXCL12 has been found to be upregulated in the cerebrospinal fluid (CSF), monocytes, plasma, and placenta during ZIKV infection [12,13,30]. To investigate the effect of inhibiting expression of this chemokine in ZIKV infection, we used a LNP to deliver siRNA in vivo to silence CXCL12 in mice infected with ZIKV. Recent studies also reported the utility of LNP to deliver siRNA as platform to treat or investigate physiological processes for therapeutic applications in cancer, cardiovascular and infection diseases [17,31].

Biodistribution analysis demonstrated that the siRNA delivered via LNPs exhibits a marked preference for accumulating in the liver and spleen. We also demonstrated that the treatment has no discernible impact on infiltrating cells in the brain, nor does it appear to exert any systemic effects on either leukocyte counts or observed symptoms in mock or ZIKV groups treated with LNP (Fig. 2). It has previously been shown that immunomodulation in the spleen could alter brain immune response during malaria infection [32]; thus, we reasoned that the inhibition of CXCL12 in the spleen could suffice to alter the inflammatory balance in the brain during ZIKV infection. In addition, CXCL12 is known to influence macrophage polarization in various microenvironments, including tumor sites, gut injuries, orthodontic tissues, and implanted biomaterials [33–38]. However, to the best of our knowledge, this influence is not well described in the context of brain immunity. Mature astrocytes (characterized by S100b expression) participate in BBB maintenance [39,40] and microglia expressing Iba1 are the immunocompetent and phagocytic cells of the nervous system [41].

Our immunofluorescence data demonstrate that the number of astrocytes and macrophages in the brain was not influenced by CXCL12 silencing (Fig. 3). However, an upregulation in expression of CD68, a lysosomal protein, was observed in ZIKV+siCXCL12-LNP group, suggestive of phagocytic activity in activated microglia (Fig. 3) [42]. To corroborate this data, activated microglia ($CD45^{int}CD11b^{+}F4/80^{+}MHCI^{+}$) were found to be more prevalent after CXCL12 silencing (Fig. 3I-J). It has been described that population of microglia expressing MHC class I and II and costimulatory molecules may arise during infectious and inflammatory conditions [25]. When activated, microglia are potent immune effector cells, able to perform a wide range of functions, and they mediate both innate and adaptive responses during disease [43]. ZIKV infection was also associated with secretion of inflammatory mediators linked with CNS inflammation such as IL-6, TNF-α, IL-1β, iNOS and NO [44]. Our FACS data demonstrated an additional increase of iNOS and TNF-α, in microglial cells after CXCL12 silencing during ZIKV infection (Fig. 4). Thus, fine modulation of microglia activation is essential for its normal function, as suggested by our pro- and anti-inflammatory data of activated microglia during ZIKV infection.

Peripheral cells can infiltrate the CNS during ZIKV infection [29,39,40]; however, we found that prevalence of $CD45^{+}$ myeloid cell subsets was not altered in the ZIKV+siCXCL12-LNP group (Fig. S3). Infiltrating T cells limit ZIKV infection [45]. We observed an increase in T cell subsets releasing IFN-ɣ and IL-17 in the brains of ZIKV infected mice. Similar findings were previously described in the serum of infected patients with ZIKV [46]. However, enhanced IFN-ɣ and IL-17 secretion was not found after CXCL12 silencing (ZIKV+siCXCL12-LNP group). These results may be explained by the fact that CXCL12 enhances stimulation

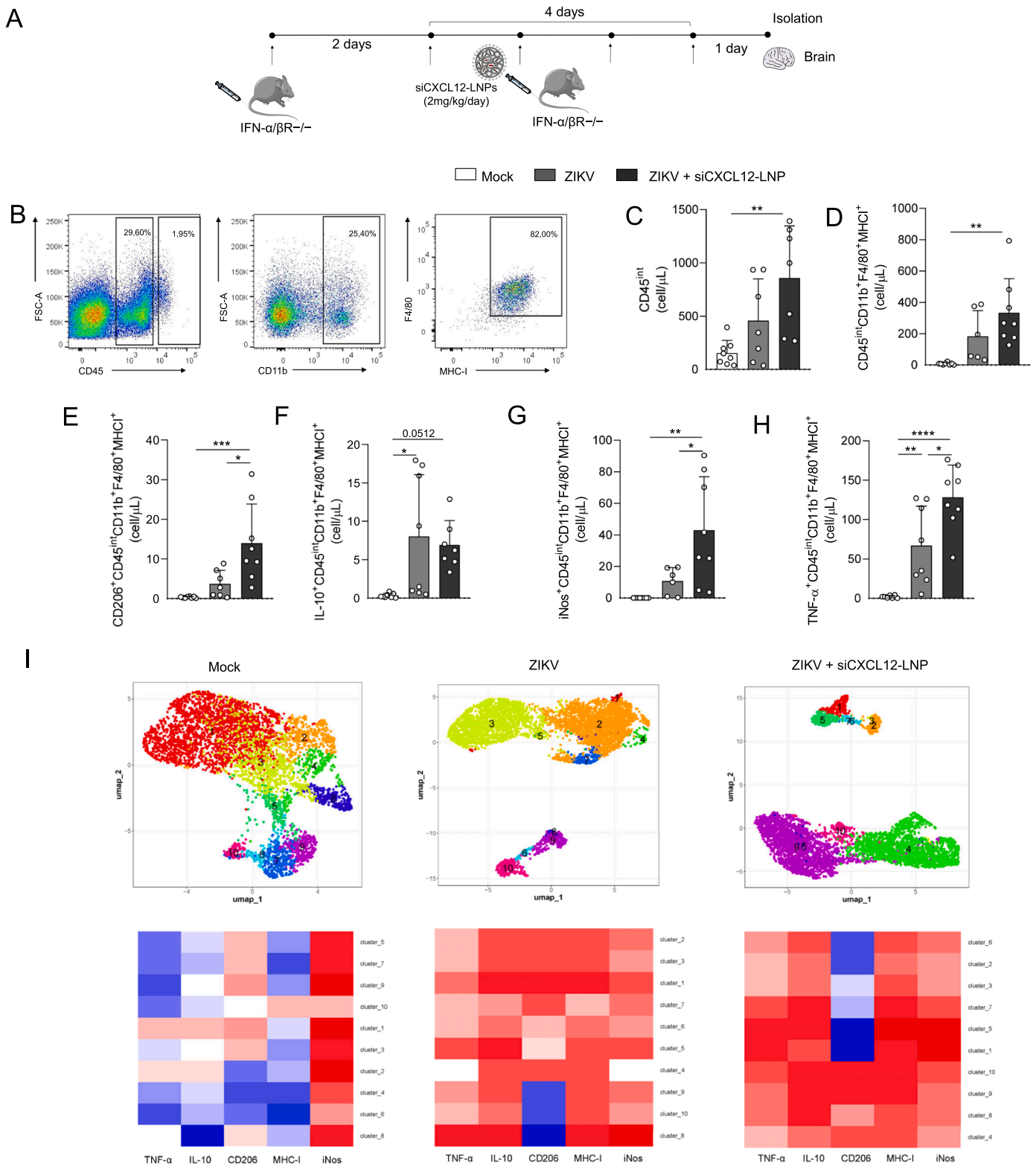

Fig. 4. Cytokine release from microglia is altered by CXCL12 silencing during ZIKV infection. (A) Representative density of ($CD45^{high}$), ($CD11b^{+}$), activated microglia ($F4/80^{+}$/MHC-I^{+}) from a single ZIKV-infected brain. Number of cells (cell/uL) of (B) $CD45^{int}$, (C) Activated microglia ($CD45^{int}CD11b^{+}F4/80^{+}MHC\text{-}1^{+}$), (D) Activated microglia expressing mannose receptor ($CD45^{int}CD11b^{+}F4/80^{+}MHC\text{-}1^{+}CD206^{+}$). Microglia producer of (E) IL-10 ($CD45^{int}CD11b^{+}F4/80^{+}MHC\text{-}1^{+}IL\text{-}10^{+}$), (F) iNOS ($CD45^{int}CD11b^{+}F4/80^{+}MHC\text{-}1^{+}iNos^{+}$) and (G) TNF-α ($CD45^{int}CD11b^{+}F4/80^{+}MHC\text{-}1^{+}TNF\text{-}\alpha^{+}$), from mock, ZIKV and ZIKV+siCXCL12-LNP groups of IFN-α/βR− /− mice (n = 24). (I) UMAP of combined data (upper panel) of mock, ZIKV and ZIKV+siCXCL12-LNP groups. Analysis was reached using the group of cells identified as activated microglia ($CD45^{int}CD11b^{+}F4/80^{+}MHC\text{-}1^{+}$). IL-10, TNF-α, CD206, MHC-I, and iNos distribution were stratified according to each group. Heatmap of CD206, and expression of different cytokines in activated microglia from mock, ZIKV, and ZIKV+siCXCL12-LNP groups (bottom panel). Data are presented as mean ± SD. One-way ANOVA followed by Tukey's multiple comparison test; * .01 < p < .05, * *.001 < p < 0.01, * ** p < 0.001, and * ** * p < 0.0001.

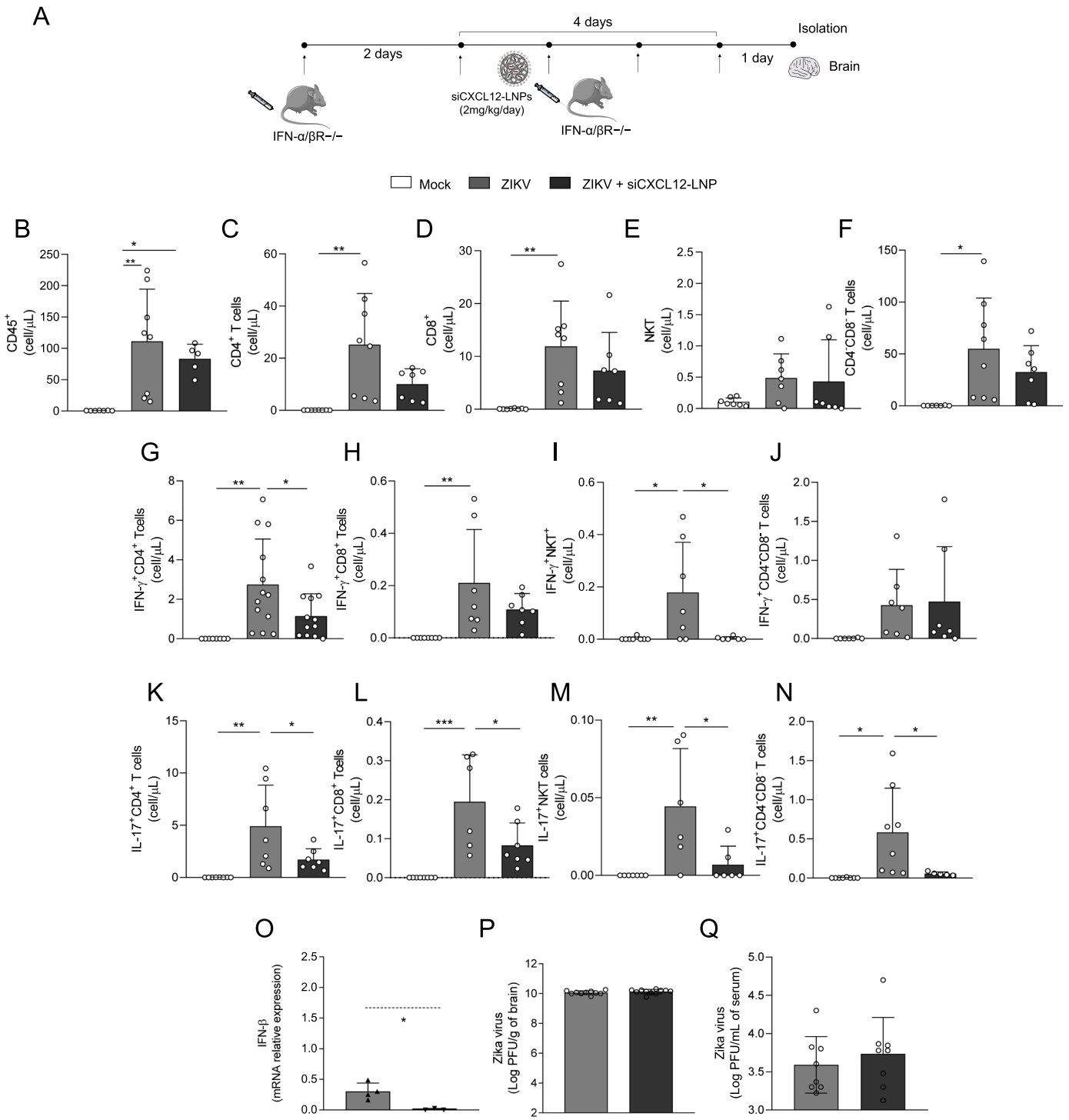

Fig. 5. T cell cytokines are modulated by CXCL12 levels during ZIKV infection. (A) Treatment protocol to assess the effect of siCXCL12 in brain. Scheme of infection with ZIKV and treatment with siCXCL12-LNPs. Brain leukocytes were analyzed in different groups: mock, ZIKV and ZIKV+siCXCL12-LNP of IFN-α/βR− /− mice (n = 24). (B) $CD45^+$ leukocytes and T cells subpopulations (C) CD4, (D) CD8, (E) $CD4^-CD8^-$T and (F) NKT were evaluated. Furthermore, (G-J) IFN-ɣ and (K-N) IL-17 production were evaluated in the same subpopulations. (O) mRNA levels of IFN-β via qRT-PCR, lines represent the mock (n = 4) and (P) viral load in the brain and (Q) serum at 6 days post-infection with ZIKV (n = 13). The results are shown as the log PFU per gram of brain or mL of serum. Data are presented as mean ± SD. (B - N) One-way ANOVA followed by Tukey's multiple comparison test and (O) Mann-Whitney test; * .01 < p < .05, * *.001 < p < 0.01, * ** p < 0.001, and p < 0.0001.

of T cells through the T cell receptor (TCR) and possesses a chemotactic ability [26]. Additionally, ZIKV infection is known to cause the down-regulation of IRF3 and antiviral NF-κB-mediated signaling, resulting in the blocking of type-I interferons [28]. Consistent with this, the impact of CXCL12 silencing on IFN-β release revealed a significant reduction in the ZIKV+siCXCL12-LNP group. The crosstalk between microglia and Th1 cells triggers an increase of type I interferon by microglia [47]. After CXCL12 silencing (ZIKV+siCXCL12-LNP group) we found decreased both IFN-ɣ and IFN-β. IFN-family cytokines are important for the clearance of ZIKV; however, the decrease of IFN-ɣ and IFN-β were evidently not enough to increase viral load at the 6th day in ZIKV+siCXCL12-LNP group, possible due to the apparently acquired

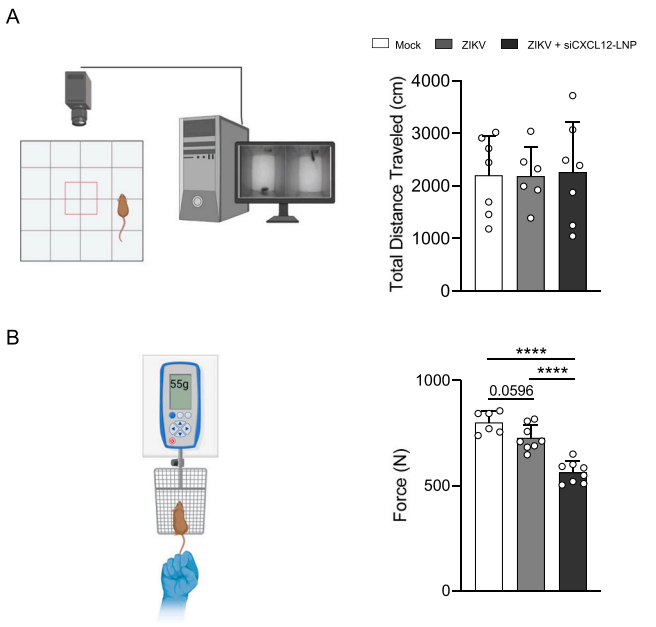

Fig. 6. Animal behavior after CXCL12 silencing during ZIKV infection. Behavioral tests were performed in different groups: mock, ZIKV and ZIKV+siCXCL12-LNP of IFN-α/βR− /− mice. (A) Scheme of open field test (left panel) and total distance traveled in cm (right panel); (B) Scheme of grip force test (left panel) and grip force of two paws (right panel) (n = 24). Data are presented as mean ± SD. One-way ANOVA followed by Tukey's multiple comparison test; * .01 < p < .05, * *.001 < p < .01, * ** p < .001 and * ** p < .0001.

viral plateau, which might have been a result of neuronal cell death triggered by increased TNF-α associated with intense virus proliferation and virion production [48,49].

It has been described the importance of CXCL12 in skeletal muscle regeneration, in particular, enhanced expression during myoblasts differentiation [50]. Here, we observed loss of grip strength after CXCL12 silencing (ZIKV+siCXCL12-LNP group), triggering adverse consequences in the absence of CXCL12 during ZIKV infection. In this work, we observed that activated infiltrated T cells decreased cytokine production in the brain after CXCL12 silencing. However, local brain immune response was upregulated with increased iNOS and TNF-α levels as well as loss of grip strength, without changes in the viral load or clinical score. Importantly, the mouse model IFN-α/βR− /− used for ZIKV establishment is a limitation of our study, since the innate immune responses are impaired.

5. Conclusion

Here, we developed a LNP to deliver siRNA in vivo to investigate the impact of CXCL12 silencing in the context of ZIKV infection. Our results demonstrated that CXCL12 silencing modulates brain immune response during ZIKV infection. We observed that brain resident cells upregulated pro-inflammatory cytokines and infiltrated T cells decreased cytokine release after CXCL12 silencing. In addition, supporting the significance of this chemokine in the context of ZIKV infection, silence triggered strength deficits. Collectively, this work introduces the potential of nanoparticle-RNA interference as a tool to investigate immune responses in the context of ZIKV infection.

CRediT authorship contribution statement

Pires Goulart Guimaraes Pedro: Conceptualization, Funding acquisition, Project administration, Resources, Supervision, Writing – original draft. **Scalzo Sérgio Ricardo Aluotto:** Data curation, Writing – review & editing. **Costa Vivian Vasconcelos:** Investigation, Project administration, Resources, Writing – review & editing. **Oliveira Bruna Silva:** Investigation, Methodology. **Fernandes Rúbia Aparecida:** Investigation, Methodology. **Santos Felipe Rocha da Silva:** Investigation, Methodology. **Hamilton Alex:** Writing – review & editing. **Costa Pedro Augusto Carvalho:** Conceptualization, Data curation, Formal analysis, Investigation, Methodology, Writing – original draft. **Palanki Rohan:** Writing – review & editing. **Santos Victor Rodrigues:** Data curation, Investigation, Methodology, Writing – review & editing. **Prazeres Pedro Henrique Dias Moura:** Investigation, Methodology. **Birbrair Alexander:** Writing – review & editing. **Silva Walison Nunes:** Data curation, Formal analysis, Methodology. **Teixeira Mauro Martins:** Resources, Writing – review & editing. **Mitchell Michael J.:** Investigation, Writing – review & editing. **Silva Natália Jordana Alves:** Data curation, Investigation, Methodology. **Miranda Aline Silva:** Investigation, Methodology, Writing – review & editing. **Ferreira Heloísa Athaydes Seabra:** Investigation, Methodology. **Figueiredo Maria Marta:** Investigation, Methodology.

Declaration of Competing Interest

The authors declare no conflict of interest.

Data availability

Data will be made available on request.

Acknowledgements

This work was funded by National Council for Scientific and Technological Development-CNPq (401390/2020-9; 442731/2020-5; 305932/2022-5; 422002/2023-2; 408482/2022-2), PRPq-UFMG, CAPES (88887.506690/2020-00), and FAPEMIG (APQ-00826–21; APQ-02402-23; RED-00202-22 Rede de Pesquisa em Imunobiológicos e Biofármacos para terapias avançadas e inovadoras). P.P.G.G. is supported by CNPq (442731/2020-5; 305932/2022-5; 422002/2023-2; 408482/2022-2) and FAPEMIG (APQ-00826-21; APQ-02402-23).

Supplementary materials

Fig. S1 - CXCL12 silencing alters IBA-1 +CD68 + cell body in the brain during ZIKV infection. Size of cell bodies of (A) IBA-1 +CD68 +DAPI and (B) S100b+DAPI. Data are presented as mean ± SD. Tukey's multiple comparison test; * .01 < p < .05, * *.001 < p < 0.01, * ** p < 0.001, and * ** * p < 0.0001.

Fig. S2 - CXCL12 silencing does not induce myeloid activation in the brain during ZIKV infection. Brain myeloid leukocytes were analyzed in different groups: mock, ZIKV and ZIKV+siCXCL12-LNP of IFN-α/βR− /− mice (n = 24). Number of (A) macrophages, (B) monocytes, and (C) dendritic cells releasing (D-F) TNF, (G-I) iNOS, (J-L) IL-10, and (M-O) expressing CD206. Data are presented as mean ± SD. One-way ANOVA followed by Tukey's multiple comparison test; * .01 < p < .05, * *.001 < p < 0.01, and * ** p < 0.001.

Fig. S3 - CXCL12 silencing does not alter Treg and NK. Brain leukocytes were analyzed in different groups: mock, ZIKV and ZIKV+siCXCL12-LNP of IFN-α/βR− /− mice (n = 24). (A) Treg cells and (B) NK were evaluated. Furthermore, (C-D) IFN-ɣ and (E-F) IL-17 production was evaluated by the same subpopulations. Data are presented as mean ± SD. One-way ANOVA followed by Tukey's multiple comparison test; * .01 < p < .05, and * *.001 < p < 0.01.

Fig. S4 - Liver optical photomicrograph. Representative histopathological images of the liver from all groups. The hydropic degeneration is focally present (red arrow), intact hepatocytes (green arrow), congested vessels (blue arrow).

Appendix A. Supporting information

Supplementary data associated with this article can be found in the online version at doi:10.1016/j.biopha.2023.115981.

References

[1] A.C. Simões-e-Silva, J.M. Moreira, R.M.C. Romanelli, A.L. Teixeira, Zika virus challenges for neuropsychiatry, Neuropsychiatr. Dis. Treat. 12 (2016) 1747–1760, https://doi.org/10.2147/NDT.S113037.

[2] J. Mlakar, M. Korva, N. Tul, M. Popović, M. Poljšak-Prijatelj, J. Mraz, M. Kolenc, K. Resman Rus, T. Vesnaver Vipotnik, V. Fabjan Vodušek, A. Vizjak, J. Pižem, M. Petrovec, T. Avšič Županc, Zika virus associated with microcephaly, N. Engl. J. Med 374 (2016) 951–958, https://doi.org/10.1056/NEJMOA1600651.

[3] V.M. Cao-Lormeau, C. Roche, A. Teissier, E. Robin, A.L. Berry, H.P. Mallet, A. A. Sall, D. Musso, Zika virus, French polynesia, South pacific, 2013, Emerg. Infect. Dis. 20 (2014) 1085–1086, https://doi.org/10.3201/EID2006.140138.

[4] F.R. Cugola, I.R. Fernandes, F.B. Russo, B.C. Freitas, J.L.M. Dias, K.P. Guimarães, C. Benazzato, N. Almeida, G.C. Pignatari, S. Romero, C.M. Polonio, I. Cunha, C. L. Freitas, W.N. Brandaõ, C. Rossato, D.G. Andrade, D.D.P. Faria, A.T. Garcez, C. A. Buchpigel, C.T. Braconi, E. Mendes, A.A. Sall, P.M.D.A. Zanotto, J.P.S. Peron, A. R. Muotri, P.C.B.B. Beltrao-Braga, The Brazilian Zika virus strain causes birth defects in experimental models, Nature 534 (2016) 267–271, https://doi.org/10.1038/NATURE18296.

[5] Zika virus disease outbreak 2015–2016, World Health Organization. (n.d.). ⟨https://www.who.int/emergencies/situations/zika-virus-outbreak⟩ (accessed January 24, 2023).

[6] Y. Acosta-Ampudia, D.M. Monsalve, L.F. Castillo-Medina, Y. Rodríguez, Y. Pacheco, S. Halstead, H.J. Willison, J.M. Anaya, C. Ramírez-Santana, Autoimmune neurological conditions associated with zika virus infection, Front Mol. Neurosci. 11 (2018), https://doi.org/10.3389/FNMOL.2018.00116.

[7] N. Zhang, N. Zhang, C.F. Qin, X. Liu, L. Shi, Z. Xu, Zika virus disrupts neural progenitor development and leads to microcephaly in mice, Cell Stem Cell 19 (2016) 120–126, https://doi.org/10.1016/J.STEM.2016.04.017.

[8] P.P. Garcez, E.C. Loiola, R.M. da Costa, L.M. Higa, P. Trindade, R. Delvecchio, J. M. Nascimento, R. Brindeiro, A. Tanuri, S.K. Rehen, Zika virus impairs growth in human neurospheres and brain organoids, Science 352 (2016) 816–818, https://doi.org/10.1126/SCIENCE.AAF6116.

[9] L.J. Lee, T.V. Komarasamy, N.A.A. Adnan, W. James, V. RMT, Balasubramaniam, hide and seek: the interplay between Zika virus and the host immune response, Front. Immunol. 12 (2021) 4379, https://doi.org/10.3389/FIMMU.2021.750365/.

[10] T.V. Komarasamy, N.A.A. Adnan, W. James, V.R.M.T. Balasubramaniam, Zika virus neuropathogenesis: the different brain cells, host factors and mechanisms involved, Front. Immunol. 13 (2022) 981, https://doi.org/10.3389/FIMMU.2022.773191/.

[11] S. Jäkel, L. Dimou, Glial cells and their function in the adult brain: a journey through the history of their ablation, Front Cell Neurosci. 11 (2017) 24, https://doi.org/10.3389/FNCEL.2017.00024/.

[12] D. Michlmayr, P. Andrade, K. Gonzalez, A. Balmaseda, E. Harris, CD14+CD16+ monocytes are the main target of Zika virus infection in peripheral blood mononuclear cells in a paediatric study in Nicaragua, Nat. Microbiol 2 (2017) 1462–1470, https://doi.org/10.1038/S41564-017-0035-0.

[13] A.T. Panganiban, R.V. Blair, J.B. Hattler, D.G. Bohannon, M.C. Bonaldo, B. Schouest, N.J. Maness, W.K. Kim, A Zika virus primary isolate induces neuroinflammation, compromises the blood-brain barrier and upregulates CXCL12 in adult macaques, Brain Pathol. 30 (2020) 1017, https://doi.org/10.1111/BPA.12873.

[14] K.A. Whitehead, R. Langer, D.G. Anderson, Knocking down barriers: advances in siRNA delivery, Nat. Rev. Drug Discov. 8 (2009) 129–138, https://doi.org/10.1038/NRD2742.

[15] H. Yin, R.L. Kanasty, A.A. Eltoukhy, A.J. Vegas, J.R. Dorkin, D.G. Anderson, Non-viral vectors for gene-based therapy, Nat. Rev. Genet 15 (2014) 541–555, https://doi.org/10.1038/NRG3763.

[16] C. Li, A. Lee, L. Grigoryan, P.S. Arunachalam, M.K.D. Scott, M. Trisal, F. Wimmers, M. Sanyal, P.A. Weidenbacher, Y. Feng, J.Z. Adamska, E. Valore, Y. Wang, R. Verma, N. Reis, D. Dunham, R. O'Hara, H. Park, W. Luo, A.D. Gitlin, P. Kim, P. Khatri, K.C. Nadeau, B. Pulendran, Mechanisms of innate and adaptive immunity to the Pfizer-BioNTech BNT162b2 vaccine, 2022 23:4, Nat. Immunol. 23 (2022) 543–555, https://doi.org/10.1038/s41590-022-01163-9.

[17] M. Krohn-Grimberghe, M.J. Mitchell, M.J. Schloss, O.F. Khan, G. Courties, P.P. G. Guimaraes, D. Rohde, S. Cremer, P.S. Kowalski, Y. Sun, M. Tan, J. Webster, K. Wang, Y. Iwamoto, S.P. Schmidt, G.R. Wojtkiewicz, R. Nayar, V. Frodermann, M. Hulsmans, A. Chung, F.F. Hoyer, F.K. Swirski, R. Langer, D.G. Anderson, M. Nahrendorf, Nanoparticle-encapsulated siRNAs for gene silencing in the haematopoietic stem-cell niche, 2020 4:11, Nat. Biomed. Eng. 4 (2020) 1076–1089, https://doi.org/10.1038/s41551-020-00623-7.

[18] V. v Costa, C.T. Fagundes, D.F. Valadão, T. v Ávila, D. Cisalpino, R.F. Rocha, L. S. Ribeiro, F.R. Ascenção, L.M. Kangussu, C.M.Q. Junior, R.G. Astigarraga, F. L. Gouveia, T.A. Silva, D. Bonaventura, D. de Almeida Sampaio, A.C.L. Leite, M. M. Teixeira, D.G. Souza, Subversion of early innate antiviral responses during antibody-dependent enhancement of Dengue virus infection induces severe disease in immunocompetent mice, Med. Microbiol. Immunol. 203 (2014) 231–250, https://doi.org/10.1007/S00430-014-0334-5.

[19] S.D. Dowall, V.A. Graham, E. Rayner, B. Atkinson, G. Hall, R.J. Watson, A. Bosworth, L.C. Bonney, S. Kitchen, R. Hewson, A susceptible mouse model for Zika virus infection, PLoS Negl. Trop. Dis. 10 (2016), e0004658, https://doi.org/10.1371/JOURNAL.PNTD.0004658.

[20] K.J. Livak, T.D. Schmittgen, Analysis of relative gene expression data using real-time quantitative PCR and the 2(-Delta Delta C(T)) Method, Methods 25 (2001) 402–408, https://doi.org/10.1006/METH.2001.1262.

[21] D.J. Donnelly, J.C. Gensel, D.P. Ankeny, N. van Rooijen, P.G. Popovich, An efficient and reproducible method for quantifying macrophages in different experimental models of central nervous system pathology, J. Neurosci. Methods 181 (2009) 36, https://doi.org/10.1016/J.JNEUMETH.2009.04.010.

[22] E.A. Bordt, C.L. Block, T. Petrozziello, G. Sadri-Vakili, C.J. Smith, A.G. Edlow, S. D. Bilbo, Isolation of microglia from mouse or human tissue, STAR Protoc. 1 (2020), 100035, https://doi.org/10.1016/J.XPRO.2020.100035.

[23] K. Grabert, B.W. McColl, Isolation and phenotyping of adult mouse microglial cells, Methods Mol. Biol. 1784 (2018) 77–86, https://doi.org/10.1007/978-1-4939-7837-3_7.

[24] V.V. Costa, J.L. Del Sarto, R.F. Rocha, F.R. Silva, J.G. Doria, I.G. Olmo, R. E. Marques, C.M. Queiroz-Junior, G. Foureaux, J.M.S. Araújo, A. Cramer, A.L.C. V. Real, L.S. Ribeiro, S.I. Sardi, A.J. Ferreir, F.S. Machado, A.C. De Oliveira, A. L. Teixeira, H.I. Nakaya, D.G. Souza, F.M. Ribeiro, M.M. Teixeira, N-Methyl-d-Aspartate (NMDA) receptor blockade prevents neuronal death induced by Zika virus infection, MBio 8 (2017), https://doi.org/10.1128/MBIO.00350-17.

[25] R.B. Rock, G. Gekker, S. Hu, W.S. Sheng, M. Cheeran, J.R. Lokensgard, P. K. Peterson, Role of microglia in central nervous system infections, Clin. Microbiol Rev. 17 (2004) 942, https://doi.org/10.1128/CMR.17.4.942-964.2004.

[26] X. Smith, H. Schneider, K. Köhler, H. Liu, Y. Lu, C.E. Rudd, The chemokine CXCL12 generates costimulatory signals in T cells to enhance phosphorylation and clustering of the adaptor protein SLP-76, Sci. Signal 6 (2013), https://doi.org/10.1126/SCISIGNAL.2004018/.

[27] J.R. Bowen, K.M. Quicke, M.S. Maddur, J.T. O'Neal, C.E. McDonald, N. B. Fedorova, V. Puri, R.S. Shabman, B. Pulendran, M.S. Suthar, Zika Virus antagonizes type I interferon responses during infection of human dendritic cells, PLoS Pathog. 13 (2017), https://doi.org/10.1371/JOURNAL.PPAT.1006164.

[28] A. Kumar, S. Hou, A.M. Airo, D. Limonta, V. Mancinelli, W. Branton, C. Power, T. C. Hobman, Zika virus inhibits type-I interferon production and downstream signaling, EMBO Rep. 17 (2016) 1766–1775, https://doi.org/10.15252/EMBR.201642627.

[29] Y. Takeshita, R.M. Ransohoff, Inflammatory cell trafficking across the blood-brain barrier (BBB): chemokine regulation and in vitro models, Immunol. Rev. 248 (2012) 228, https://doi.org/10.1111/J.1600-065X.2012.01127.X.

[30] F. Gambino, W. Tai, D. Voronin, Y. Zhang, X. Zhang, J. Shi, X. Wang, N. Wang, L. Du, L. Qiao, A vaccine inducing solely cytotoxic T lymphocytes fully prevents Zika virus infection and fetal damage, Cell Rep. 35 (2021), https://doi.org/10.1016/J.CELREP.2021.109107.

[31] P.P.G. Guimarães, C.G. Figueroa-Espada, R.S. Riley, N. Gong, L. Xue, T. Sewastianik, P.S. Dennis, C. Loebel, A. Chung, S.J. Shepherd, R.M. Haley, A. G. Hamilton, R. El-Mayta, K. Wang, R. Langer, D.G. Anderson, R.D. Carrasco, M. J. Mitchell, In vivo bone marrow microenvironment siRNA delivery using lipid–polymer nanoparticles for multiple myeloma therapy, Proc. Natl. Acad. Sci. 120 (2023), e2215711120, https://doi.org/10.1073/PNAS.2215711120.

[32] B.S. Franklin, S.T. Ishizaka, M. Lamphier, F. Gusovsky, H. Hansen, J. Rose, W. Zheng, M.A. Ataíde, R.B. De Oliveira, D.T. Golenbock, R.T. Gazzinelli, Therapeutical targeting of nucleic acid-sensing Toll-like receptors prevents experimental cerebral malaria, Proc. Natl. Acad. Sci. 108 (2011), https://doi.org/10.1073/pnas.1015406108.

[33] S. Babazadeh, S.M. Nassiri, V. Siavashi, M. Sahlabadi, M. Hajinasrollah, M. Zamani-Ahmadmahmudi, Macrophage polarization by MSC-derived CXCL12 determines tumor growth, Cell Mol. Biol. Lett. 26 (2021) 1–15, https://doi.org/10.1186/S11658-021-00273-W/.

[34] X.Y. Fang, Y.X. Zhan, X.M. Zhou, L.N. Wu, J. Lin, Y.T. Yi, C.M. Jiang, J. Wang, J. Liu, CXCL12/CXCR4 mediates orthodontic root resorption via regulating the M1/M2 ratio, J. Dent. Res 101 (2022) 569–579, https://doi.org/10.1177/00220345211050324.

[35] L. Sá Nchez-Martín, A. Estecha, R. Samaniego, S. Sá Nchez-Ramón, M.Á. Ngel Vega, P. Sá Nchez-Mateos, The chemokine CXCL12 regulates monocyte-macrophage differentiation and RUNX3 expression, Blood (2011), https://doi.org/10.1182/blood-2009-12-258186.

[36] X. Cai, R. Chen, K. Ma, F. Wang, Y. Zhou, Y. Wang, T. Jiang, Identification of the CXCL12–CXCR4/CXCR7 axis as a potential therapeutic target for immunomodulating macrophage polarization and foreign body response to implanted biomaterials, Appl. Mater. Today 18 (2020), 100454, https://doi.org/10.1016/J.APMT.2019.100454.

[37] P. Ruytinx, P. Proost, J. Van Damme, S. Struyf, Chemokine-induced macrophage polarization in inflammatory conditions, Front Immunol. 9 (2018) 1930, https://doi.org/10.3389/FIMMU.2018.01930/.

[38] J. Giri, R. Das, E. Nylen, R. Chinnadurai, J.G. Correspondence, CCL2 and CXCL12 derived from mesenchymal stromal cells cooperatively polarize IL-10+ tissue macrophages to mitigate gut injury, Tissue Macrophages Mitigate Gut Inj., Cell. 30 (2020) 1923–1934.e4, https://doi.org/10.1016/j.celrep.2020.01.047.

[39] H.K. Kimelberg, Functions of mature mammalian astrocytes: a current view, Neuroscientist 16 (2010) 79–106, https://doi.org/10.1177/1073858409342593.

[40] E. Raponi, F. Agenes, C. Delphin, N. Assard, J. Baudier, C. Legraverend, J. C. Deloulme, S100B expression defines a state in which GFAP-expressing cells lose their neural stem cell potential and acquire a more mature developmental stage, Glia 55 (2007) 165, https://doi.org/10.1002/GLIA.20445.

[41] W. Enlow, M. Bordeleau, J. Piret, F.G. Ibáñez, O. Uyar, M.C. Venable, N. Goyette, J. Carbonneau, M.E. Tremblay, G. Boivin, Microglia are involved in phagocytosis

and extracellular digestion during Zika virus encephalitis in young adult immunodeficient mice, J. Neuroinflamm. 18 (2021) 1–24, https://doi.org/10.1186/S12974-021-02221-Z/.

[42] D. Beckman, A.M.H. Seelke, J. Bennett, P. Dougherty, K.K.A. van Rompay, R. Keesler, P.A. Pesavento, La.L.A. Coffey, J.H. Morrison, E. Bliss-Moreau, Neuroanatomical abnormalities in a nonhuman primate model of congenital Zika virus infection, Elife 11 (2022) 64734, https://doi.org/10.7554/ELIFE.64734.

[43] Q. Li, B.A. Barres, Microglia and macrophages in brain homeostasis and disease, 2017 18:4, Nat. Rev. Immunol. 18 (2017) 225–242, https://doi.org/10.1038/nri.2017.125.

[44] F. Diop, T. Vial, P. Ferraris, S. Wichit, M. Bengue, R. Hamel, L. Talignani, F. Liegeois, J. Pompon, H. Yssel, G. Marti, D. Missé, Zika virus infection modulates the metabolomic profile of microglial cells, PLoS One 13 (2018), https://doi.org/10.1371/JOURNAL.PONE.0206093.

[45] K.A. Jurado, L.J. Yockey, P.W. Wong, S. Lee, A.J. Huttner, A. Iwasaki, Antiviral CD8 T cells induce Zika virus associated paralysis in mice, Nat. Microbiol 3 (2018) 141, https://doi.org/10.1038/S41564-017-0060-Z.

[46] F.G. Naveca, G.S. Pontes, A.Y.H. Chang, G.A.V. da Silva, V.A. do Nascimento, D.C. da S. Monteiro, M.S. da Silva, L.F. Abdalla, J.H.A. Santos, T.A.P. de Almeida, M. del C.C. Mejía, T.G.R. de Mesquita, H.V. de S. Encarnação, M. de S. Gomes, L. R. Amaral, A.C. Campi-Azevedo, J.G. Coelho-Dos-Reis, L.R. do V. Antonelli, A. Teixeira-Carvalho, O.A. Martins-Filho, R. Ramasawmy, Analysis of the immunological biomarker profile during acute Zika virus infection reveals the overexpression of CXCL10, a chemokine linked to neuronal damage, Mem. Inst. Oswaldo Cruz 113 (2018), https://doi.org/10.1590/0074-02760170542.

[47] C. Benakis, A. Simats, S. Tritschler, S. Heindl, S. Besson-Girard, G. Llovera, K. Pinkham, A. Kolz, A. Ricci, F.J. Theis, S. Bittner, Ö. Gökce, A. Peters, A. Liesz, T cells modulate the microglial response to brain ischemia, Elife 11 (2022), https://doi.org/10.7554/ELIFE.82031.

[48] F. Cheng, S.R. da Silva, I.-C. Huang, J.U. Jung, S.-J. Gao, Suppression of Zika Virus Infection and Replication in Endothelial Cells and Astrocytes by PKA Inhibitor PKI 14-22, J. Virol. 92 (2018), https://doi.org/10.1128/JVI.02019-17.

[49] U. Neniskyte, A. Vilalta, G.C. Brown, Tumour necrosis factor alpha-induced neuronal loss is mediated by microglial phagocytosis, FEBS Lett. (2014), https://doi.org/10.1016/j.febslet.2014.05.046.

[50] E. Brzoska, M. Kowalewska, A. Markowska-Zagrajek, K. Kowalski, K. Archacka, M. Zimowska, I. Grabowska, A.M. Czerwińska, M. Czarnecka-Góra, W. Stremińska, K. Jańczyk-Ilach, M.A. Ciemerych, Sdf-1 (CXCL12) improves skeletal muscle regeneration via the mobilisation of Cxcr4 and CD34 expressing cells, Biol. Cell 104 (2012) 722–737, https://doi.org/10.1111/BOC.201200022.